Proton-gated Ca^{2+}-permeable TRP channels mediate myelin damage in ischaemia

Nicola B. Hamilton, Karolina Kolodziejczyk, Eleni Kougioumtzidou & David Attwell

Department of Neuroscience, Physiology & Pharmacology,

University College London, Gower St., London, WC1E 6BT, UK

Address correspondence to David Attwell, d.attwell@ucl.ac.uk

Karolina Kolodziejczyk's current address is Dept. of Psychiatry, University of British

Columbia, 2255 Wesbrook Mall, Vancouver, BC V6T 1Z3, Canada

The myelin sheaths wrapped around axons by oligodendrocytes are crucial for brain function. In ischaemia myelin is damaged in a Ca^{2+}-dependent manner, abolishing action potential propagation[1,2]. This has been attributed to glutamate release activating Ca^{2+}-permeable NMDA receptors[2-4]. Surprisingly, we now show that NMDA does not raise $[Ca^{2+}]_i$ in mature oligodendrocytes and that, although ischaemia evokes a glutamate-triggered membrane current[4], this is generated by a rise of extracellular $[K^+]$ and decrease of membrane K^+ conductance. Nevertheless, ischaemia raises oligodendrocyte $[Ca^{2+}]_i$, $[Mg^{2+}]_i$ and $[H^+]_i$, and buffering intracellular pH reduces the $[Ca^{2+}]_i$ and $[Mg^{2+}]_i$ increases, showing that these are evoked by the rise of $[H^+]_i$. The H^+-gated $[Ca^{2+}]_i$ elevation is mediated by channels with characteristics of TRPA1, being inhibited by ruthenium red, isopentenyl pyrophosphate, HC-030031, A967079 or TRPA1 knockout. TRPA1 block reduces myelin damage in ischaemia. These data suggest TRPA1-containing ion channels as a therapeutic target in white matter ischaemia.

Ischaemia blocks action potential propagation through myelinated axons[1]. Electron microscopy[2] and imaging of dye-filled oligodendrocytes[3] show ischaemia-evoked Ca^{2+}-dependent damage to the capacitance-reducing myelin sheaths, which causes loss of action potential propagation. Glutamate receptor block reduces myelin damage and action potential loss[2-7], and glutamate evokes a membrane current in oligodendrocytes mediated by AMPA/kainate and NMDA receptors[2-4]. Thus, oligodendrocyte damage is thought to be excitotoxic: as for neurons in ischaemia, a rise of glutamate concentration[8] caused by reversal of glutamate transporters in oligodendrocytes and axons[9,10] activates receptors that raise[2] oligodendrocyte $[Ca^{2+}]_i$, thus damaging the cells.

However, although AMPA/KA and NMDA receptors regulate oligodendrocyte precursor development[11,12], these receptors are down-regulated as the cells mature[13-15]. How can mature oligodendrocytes be damaged excitotoxically, if they express low levels of glutamate receptors? To investigate how oligodendrocyte $[Ca^{2+}]_i$ is raised in ischaemia, we

characterised ischaemia-evoked membrane current and $[Ca^{2+}]_i$ changes in cerebellar white matter oligodendrocytes.

Solution mimicking ischaemia (see Methods) evoked an increasing inward current in oligodendrocytes (Fig. 1a-b), often with a faster phase that was obscured when responses in many cells were averaged (Fig. 1c). When applied from before the ischaemia, NBQX and D-AP5 reduced the ischaemia-evoked current by 66% (Fig. 1c-d), while mGluR block had no effect (Ext. Data Fig. 1a). Preloading for 30 mins with the glutamate transport blocker PDC, to prevent ischaemia-evoked glutamate release by reversal of transporters in the white[9] and grey[16] matter, also reduced the inward current (by 68%, Fig. 1c-d), while blocking other candidate release mechanisms had no effect (Ext. Data Fig. 1a). Thus, glutamate release by reversed uptake helps to trigger the ischaemia-evoked current. Strikingly, however, current flow through glutamate receptors generates only a small fraction of the sustained inward current evoked by ischaemia, since applying NBQX and D-AP5 from 200 sec after ischaemia had started produced only a non-significant 21% suppression of the ischaemia-evoked inward current (Fig. 1d).

In neurons, an ischaemia-evoked inward current triggered by glutamate release, but maintained by non-glutamatergic mechanisms, generates the "Extended Neuronal Depolarization" (END) that evokes neuronal death[17]. However, the ischaemia-evoked current in oligodendrocytes was not prevented by removing external Ca^{2+}, nor by gadolinium, which both block the END[17] (Fig. 1d-e), implying a different mechanism maintains the inward current triggered by glutamate.

Unlike in neurons, where ischaemia evokes a conductance increase mediated by ionotropic glutamate receptors[16], ischaemia decreased the conductance of oligodendrocytes (Fig. 1f-g). The suppressed current reversed below the K^+ reversal potential (E_K=-104 mV), at -121 mV with 10 mM (Fig. 1f, Ext. Data Fig. 1e) and -118 mV with 0.5 mM HEPES (Fig. 1g). This is expected if ischaemia decreases the membrane K^+ conductance, while $[K^+]_o$ rises (due to Na^+/K^+ pump inhibition throughout the slice) which increases the inward current at all potentials (see Ext. Data Fig. 1b-d; Suppl. Information). K^+-sensitive electrodes showed that

3

$[K^+]_o$ in the white matter initially rose slowly during ischaemia, but then increased more abruptly, in parallel with the membrane current (Fig. 1h). The peak rise was 2.35 ± 0.13 mM (n=12) in the white matter and 2.48 ± 0.35 mM (n=4) in the adjacent grey matter (where it reflects the anoxic depolarization of neurons[18]). The conductance decrease described above produced 32%, while the $[K^+]_o$ rise produced 68%, of the inward current in oligodendrocytes at -74mV (see Suppl. Information). Thus, changes in K^+ fluxes generate the ischaemia-evoked inward current.

Could part of the NMDA-evoked inward current in oligodendrocytes[4] also reflect a $[K^+]_o$ rise? Extracellular Cs^+ blocked the NMDA-evoked current while intracellular MK-801 had no effect (Ext. Data Fig. 2a-d), suggesting most of the NMDA-evoked current is generated by $[K^+]_o$ rising, rather than by oligodendrocyte NMDA receptors. Applying NMDA or raising $[K^+]_o$, and correlating the resulting inward current with the $[K^+]_o$ rise occurring (see Supplementary Information; Ext. Data Fig. 2e-f), we found that at least 49% of the NMDA-evoked current was attributable to the $[K^+]_o$ rise that it produced. Since mature oligodendrocytes express few NMDA receptors[13-15], this presumably reflects NMDA depolarizing neurons or astrocytes in the slice and releasing K^+.

These data challenge the idea[2-5] that, during ischaemia, NMDA receptors in mature oligodendrocytes generate a prolonged calcium influx which damages the cells. We therefore investigated the ion concentration changes evoked in oligodendrocytes by activation of NMDA receptors, using Ca^{2+}-, Na^+- and K^+-sensitive dyes loaded into cells from the pipette. When 100 μM NMDA was applied to whole-cell clamped cerebellar granule neurons at -74 mV, as expected it evoked an inward current, and raised $[Ca^{2+}]_i$ and $[Na^+]_i$ (Ext. Data Fig. 3). In contrast, although NMDA evoked an inward current in oligodendrocytes, it generated no $[Ca^{2+}]_i$ or $[Na^+]_i$ elevation, indeed $[Na^+]_i$ decreased after applying NMDA (Fig. 2a). NMDA raised $[K^+]_i$ however. Similar concentration changes were seen at the soma (Fig. 2a) and in the internodal processes where NMDA receptors may be located[2-4] (Fig. 2b). Like NMDA, raising $[K^+]_o$ lowered $[Na^+]_i$ (Fig. 2a, b). A likely explanation is that NMDA raises $[K^+]_o$ (Fig. 2c), which decreases $[Na^+]_i$ by activating the Na^+/K^+ pump.

The absence of a rise of $[Ca^{2+}]_i$ and $[Na^+]_i$ is surprising if oligodendrocytes express NMDA receptors[2-4]. Conceivably NMDA receptors might pass ions into a compartment in their myelinating processes which only certain Ca^{2+}-sensing dyes such as X-Rhod-1 can access[2]. However, whether X-Rhod-1 was loaded as an acetoxymethyl ester[2] or from the pipette, we observed no NMDA-evoked change of $[Ca^{2+}]_i$ in the myelinating processes (Fig. 2d). Nevertheless, we could detect spontaneous $[Ca^{2+}]_i$ rises propagating through myelinating processes in 55% of oligodendrocytes (Fig. 2e).

To confirm that ischaemia raises[2] oligodendrocyte $[Ca^{2+}]_i$, we loaded the Ca^{2+}-sensing dye Fluo-4 (with Alexa Fluor 594, for ratiometric imaging) into oligodendrocytes from a whole-cell pipette (in current-clamp mode, allowing voltage changes, in case voltage-gated Ca^{2+} channels raise $[Ca^{2+}]_i$). Ischaemia increased $[Ca^{2+}]_i$ in the soma and processes over ~10 mins. This was abolished if extracellular calcium was removed (Fig. 3a-b), and reduced by removing external K^+ (Fig. 3c), suggesting that the ischaemia-evoked $[K^+]_o$ rise promotes calcium entry from the extracellular solution. However, contradicting the earlier report[2], blocking NMDA receptors with MK-801, D-AP5 and 7-chloro-kynurenate, or blocking NMDA and AMPA/KA receptors with NBQX and D-AP5 while blocking voltage-gated Na^+ and Ca^{2+} channels and $GABA_A$ receptors, did not prevent the $[Ca^{2+}]_i$ rise (Fig. 3a-b). Similarly, when PDC-preloading reduced transporter-mediated glutamate release, the $[Ca^{2+}]$ rise was unaffected (Fig. 3c).

Similar experiments using a Mg^{2+}-sensitive dye revealed that $[Mg^{2+}]_i$ also rises in ischaemia (Fig. 3d). This was not due to ATP breakdown, which releases Mg^{2+}, since the $[Mg^{2+}]_i$ rise was abolished by removing extracellular Mg^{2+} (Fig. 3d) implying that Mg^{2+} enters across the cell membrane. Surprisingly, ischaemia did not raise $[Na^+]_i$ (Fig. 3e). Thus ischaemia activates a membrane conductance that allows entry of divalent ions.

Seeking an agent that decreases membrane K^+ conductance and activates Ca^{2+} entry, we measured the ischaemia-evoked pH change in oligodendrocytes. Ischaemia increased $[H^+]_i$ on the timescale seen for $[Ca^{2+}]_i$ (Fig. 3f). A similar (but smaller) $[H^+]_i$ rise was evoked by elevated $[K^+]_o$ or NMDA (Ext. Data Fig. 4a), suggesting that the ischaemia-evoked $[K^+]_o$ rise

partly generates this pH change. To investigate this, we removed external K^+, which reduced the $[K^+]_o$ in the slice from 2.46 ± 0.02 mM (n=13) to 0.99 ± 0.3 mM (n=4) (Mann-Whitney p=0.001, Fig. 3g), and hyperpolarized the resting potential by 7 mV (-84.0 ± 4.7 to -77.2 ± 4.3 mV, n=4, p=0.002, paired t-test, Fig. 3g). The ischaemia-evoked $[K^+]_o$ rise and depolarization were unaffected by K^+ removal (Fig. 3g), but the $[H^+]_i$ initially and during ischaemia were reduced (Fig. 3h). These data and those in Fig. 3c suggest that the ischaemia-evoked $[K^+]_o$ rise helps to acidify the cell, which in turn evokes Ca^{2+} entry.

Using an internal solution containing 50 mM HEPES, the ischaemia-evoked rise of $[H^+]_i$ was, as expected, greatly reduced (Fig. 3f). This prevented the decrease of K^+ conductance (Figs. 1g, 3i), consistent with intracellular acidity suppressing activity of tonically-active K^+ channels[19]. Strikingly, however, buffering intracellular pH also prevented the ischaemia-evoked rise of $[Ca^{2+}]_i$ and $[Mg^{2+}]_i$ (Fig. 3j-k), implying that the ischaemia-evoked $[H^+]_i$ rise activates entry of these cations into the cell. Consistent with this, uncaging protons in oligodendrocytes raised $[Ca^{2+}]_i$ and $[Mg^{2+}]_i$ (Fig. 3l-m).

Few channels allow entry of Ca^{2+} and Mg^{2+} better than Na^+, but many TRP channels share this property[20] (and TRP channel activation can cause ischaemic damage to neurons[21] and astrocytes[22]). Of these channels, only[20,23,24] TRPA1 and TRPV3 are known to be activated by intracellular H^+, so we applied modulators of these channels and examined the effect on oligodendrocyte $[Ca^{2+}]_i$ (TRP agonist and blocker specificity are discussed in Supplementary Information). The TRPA1/TRPV3 blocker isopentenyl pyrophosphate[25] (IPP) and the TRPA1 blocker[26] HC-030031 slowed and reduced the $[Ca^{2+}]_i$ rise evoked by uncaging H^+ in the cell (Fig. 3l). The TRPA1/TRPV3 agonists[20,27] menthol, vanillin, carvacrol (Cv) and 2-APB all raised $[Ca^{2+}]_i$ in oligodendrocyte somata and myelinating processes, as did the TRPA1 agonists[27] AITC, polygodial and flufenamic acid, while the TRPV3 agonists[20,27] camphor and farnesyl pyrophosphate (FPP) did not (Fig. 4a-b). Thus, TRPA1 subunit-including channels contribute to these responses, but TRPV3 channels are not needed. The carvacrol-evoked rise of $[Ca^{2+}]_i$ was reduced by HC-030031 which blocks TRPA1 but not TRPV3[26], by the TRPA1/TRPV3 blocker isopentenyl pyrophosphate[25] (IPP), and by TRPA1 knock-out (Fig

4b), again implying involvement of TRPA1 channels. It was unaffected by buffering $[H^+]_i$ (Fig. 4b), consistent with Ca^{2+} entry via TRPA1 being downstream of the $[H^+]_i$ rise, as seen with H^+ uncaging (Fig. 3l).

Using *in situ* hybridization, a TRPA1 probe labelled cerebellar white matter in rat and mouse, while a TRPV3 probe labelled rat only (Ext. Data Fig. 5a). Immunocytochemistry revealed that TRPA1- and TRPV3-expressing cells included myelinating oligodendrocytes expressing Olig2 and CC1 (Ext. Data Fig. 5b-d).

Consistent with ischaemia raising $[Ca^{2+}]_i$ by activating TRPA1- rather than TRPV3- containing channels, the general TRP blockers[20,27] ruthenium red (RuR, 10 μM) and La^{3+} (1 mM) and the TRPA1/TRPV3 blocker[25] IPP (200 μM) reduced the $[Ca^{2+}]_i$ rise, as did HC-030031 and A967079, which block TRPA1 but not TRPV3[26,28] (Fig. 4c-e). Knock-out of TRPA1 slowed and halved the ischaemia-evoked $[Ca^{2+}]_i$ rise, and the TRPA1/TRPV3 blocker IPP produced no further reduction in the knock-out (suggesting no contribution of TRPV3: Fig. 4f), while knock-out of TRPV3 did not affect the $[Ca^{2+}]_i$ rise, and the TRPA1 blocker HC-030031 slowed and halved the rise occurring in the TRPV3 knock-out (Fig 4g). Blockers of many other TRP channels had no effect (Ext. Data Fig. 6). Thus TRPA1 is the dominant contributor to the ischaemia-evoked rise of $[Ca^{2+}]_i$ in oligodendrocytes.

The larger (70%) block of the ischaemia-evoked $[Ca^{2+}]_i$ rise by the TRPA1 blocker HC-030031 than by TRPA1 knock-out (50%: Figs. 4e-f) suggests there may be compensatory upregulation of another Ca^{2+} entry pathway in the TRPA1 knock-out, which normally generates only ~30% of the $[Ca^{2+}]_i$ rise. Introducing high pH-buffering-power solution into the cell blocked the $[Ca^{2+}]_i$ rise in the TRPA1 knock-out (Fig. 4h), implying that the non-TRPA1 Ca^{2+} entry pathway is also H^+-activated. Since the non-specific TRP blockers RuR and La^{3+} abolished the ischaemia-evoked $[Ca^{2+}]_i$ rise, these data suggest there is another Ca^{2+}-permeable TRP channel (neither TRPA1 nor TRPV3) which is activated by internal H^+ in oligodendrocytes and generates ~30% of the ischaemia-evoked $[Ca^{2+}]_i$ rise.

7

To assess the role of TRPA1-containing channels in evoking myelin damage, we exposed rat optic nerves to 60 mins ischaemia. This led to disruption of myelin sheaths[2,3], which we quantified by counting the regions of myelin decompaction (lamellar separation) per axon cross section (see Methods). Taking as baseline the level of decompaction which occurs in control nerves during processing for EM, ischaemia increased decompaction ($p=3 \times 10^{-8}$), and ruthenium red or the TRPA1 blockers HC-030031 and A967079 (applied together) reduced this increase by 69% ($p=3 \times 10^{-5}$) and 59% ($p=2.0 \times 10^{-5}$) respectively (Fig. 4i-j). Ischaemia did not affect the axon g ratio (Fig. 4k: see Methods), but increased axon diameter via swelling (Fig. 4l). It also caused some axon vacuolization (Fig. 4m): vacuoles were seen in 4.3% of 2390 control axons, but in 21% of 15976 axons after ischaemia. Vacuolization was not prevented by TRP channel block (Fig. 4m), suggesting different mechanisms for axon and myelin damage.

Thus, ischaemic damage to oligodendrocytes differs fundamentally from that in neurons (Ext. Data Fig. 7), where $[Ca^{2+}]_i$ is raised by glutamate-gated receptors (and later by TRP channels activated by reactive oxygen species[21]). Contradicting current ideas[2-4], ischaemia does not damage oligodendrocytes by activating Ca^{2+} entry through ionotropic glutamate receptors in their membranes. Instead, ischaemia-evoked sodium pump inhibition and glutamate release evoke a long-lasting rise of $[K^+]_o$ that, together with metabolic changes, acidifies the oligodendrocyte, activating H^+-gated TRP channels through which Ca^{2+} enters.

In the optic nerve, ischaemia-evoked Ca^{2+} entry into oligodendrocytes is blocked by NMDA receptor antagonists[2], contradicting our demonstrations that NMDA evokes no $[Ca^{2+}]_i$ rise in oligodendrocytes (Fig. 2) and that the ischaemia-evoked $[Ca^{2+}]_i$ rise is unaffected by NMDA receptor blockers (Fig. 3). Conceivably, in the optic nerve, NMDA receptors on astrocytes[29] make a greater contribution than in cerebellum to generating the ischaemia-evoked rise of $[K^+]_o$ and thus the $[Ca^{2+}]_i$ rise.

TRPA1 generates ~70% of the ischaemia-evoked $[Ca^{2+}]_i$ rise, and TRPA1 blockers reduce ischaemic damage to myelin (Fig. 4). Consequently, blocking oligodendrocyte TRPA1-containing channels may reduce myelin loss during the energy deprivation that

follows stroke, secondary ischaemia caused by spinal cord injury, or hypoxia in multiple sclerosis[30].

References

1. Stys, P.K., Ransom,, B.R., Waxman, S.G. & Davis, P.K. Role of extracellular calcium in anoxic injury of central white matter. *Proc. Natl. Acad, Sci. USA* **87**, 4212-4216 (1990).

2. Micu, I. et al. NMDA receptors mediate calcium accumulation in myelin during chemical ischaemia. *Nature* **439**, 988-992 (2006).

3. Salter, M.G. & Fern, R. NMDA receptors are expressed in developing oligodendrocyte processes and mediate injury. *Nature* **438**, 1167-1171 (2005).

4. Káradóttir, R., Cavelier, P., Bergersen, L.H. & Attwell, D. NMDA receptors are expressed in oligodendrocytes and activated in ischaemia. *Nature* **438**, 1162-1168 (2005).

5. Bakiri, Y., Hamilton, N.B., Karadottir, R. & Attwell, D. Testing NMDA receptor block as a therapeutic strategy for reducing ischaemic damage to CNS white matter. *Glia* **56**, 233-240 (2008).

6. McCarran, W.J. & Goldberg, M.P. White matter axon vulnerability to AMPA/kainate receptor-mediated ischemic injury is developmentally regulated. *J. Neurosci.* **27**, 4220-4229 (2007).

7. Agrawal, S.K. & Fehlings, M.G. Role of NMDA and non-NMDA ionotropic glutamate receptors in traumatic spinal cord axonal injury. *J. Neurosci.* **17**, 1055-1063 (1997).

8. Sarrafzadeh, A.S., Kiening, K.L., Callsen, T.A. & Unterberg, A.W. Metabolic changes during impending and manifest cerebral hypoxia in traumatic brain injury. *Brit. J. Neurosurg.* **17**, 340-346 (2003).

9. Li, S., Mealing, G.A., Morley, P. & Stys, P.K. Novel injury mechanism in anoxia and trauma of spinal cord white matter: glutamate release via reverse Na^+-dependent glutamate transport. *J Neurosci* **19**, RC16 (1999).

10. Back, S.A. et al. Hypoxia-ischemia preferentially triggers glutamate depletion from oligodendroglia and axons in perinatal cerebral white matter. *J. Cereb. Blood Flow Metab.* **27**, 334–347 (2007).

11. Yuan, X., Eisen, A.M., McBain, C.J. & Gallo, V. A role for glutamate and its receptors in the regulation of oligodendrocyte development in cerebellar tissue slices. *Development* **125**, 2901-2914 (1998).

12. Lundgaard, I. *et al.* Neuregulin and BDNF induce a switch to NMDA receptor-dependent myelination by oligodendrocytes. *PLoS Biol.* **11**, e1001743 (2013).

13. Cahoy, J.D. et al. A transcriptome database for astrocytes, neurons, and oligodendrocytes: a new resource for understanding brain development and function. *J. Neurosci.* **28**, 264-278 (2008).

14. De Biase, L.M., Nishiyama, A. & Bergles, D.E. Excitability and synaptic communication within the oligodendrocyte lineage. *J. Neurosci.* **30**, 3600-3611 (2010).

15. Kukley, M., Nishiyama, A. & Dietrich, D. The fate of synaptic input to NG2 glial cells: neurons specifically downregulate transmitter release onto differentiating oligodendroglial cells. *J. Neurosci.* **30**, 8320-8331 (2010).

16. Rossi, D.J., Oshima, T. & Attwell, D. Glutamate release in severe brain ischaemia is mainly by reversed uptake. *Nature* **403**, 316-321 (2000).

17. Limbrick, D.D. Jr., Sombati, S. & DeLorenzo, R.J. Calcium influx constitutes the ionic basis for the maintenance of glutamate-induced extended neuronal depolarization associated with hippocampal neuronal death. *Cell Calcium* **33**, 69-81 (2003).

18. Hamann, M., Rossi, D.J., Mohr, C., Andrade, A.L. & Attwell, D. The electrical response of cerebellar Purkinje neurons to simulated ischaemia. *Brain* **128**, 2408-2420 (2005).

19. Lesage, F. et al. TWIK-1, a ubiquitous human weakly inward rectifying K^+ channel with a novel structure. *EMBO J.* **15**, 1004-1011 (1996).

20. Nilius, B. & Szallasi, A. Transient receptor potential channels as drug targets: from the science of basic research to the art of medicine. *Pharmacol. Rev.* **66**, 676-814 (2014).

21. Aarts, M. et al. A key role for TRPM7 channels in anoxic neuronal death. *Cell* **115**, 863-877 (2003).

22. Butenko, O. et al. The increased activity of TRPV4 channel in the astrocytes of the adult rat hippocampus after cerebral hypoxia/ischemia. *PLoS One* **7**, e39959 (2012).

23. Wang, Y.Y., Chang, R.B. & Liman, E.R. TRPA1 is a component of the nociceptive response to CO_2. *J. Neurosci.* **30**, 12958-12963 (2010).

24. Cao, X., Yang, F., Zheng, J. & Wang, K. Intracellular proton-mediated activation of TRPV3 channels accounts for the exfoliation effect of α-hydroxyl acids on keratinocytes. *J. Biol. Chem.* **31**, 25905-25916 (2012).

25. Bang, S., Yoo, S., Yang, T.J., Cho, H. & Hwang, S.W. Isopentenyl pyrophosphate is a novel antinociceptive substance that inhibits TRPV3 and TRPA1 ion channels. *Pain* **152**, 1156-1164 (2011).

26. McNamara, C.R. et al. TRPA1 mediates formalin-induced pain. *Proc. Natl. Acad. Sci. U.S.A.* **104**, 13525-13530 (2007).

27. Clapham, D.E. SnapShot: Mammalian TRP channels. *Cell* **129**, 220.e1-2 (2007).

28. Chen, J. et al. Selective blockade of TRPA1 channel attenuates pathological pain without altering noxious cold sensation or body temperature regulation. *Pain*, **152**, 1165-1172 (2011).

29. Hamilton, N.B. et al. Mechanisms of ATP- and glutamate-mediated calcium signaling in white matter astrocytes. *Glia* **56**, 734-749 (2008).

30. Davies, A.L. et al. Neurological deficits caused by tissue hypoxia in neuroinflammatory disease. *Ann. Neurol.* **74**, 815-825 (2013).

Supplementary Information is linked to the online version of the paper at www.nature.com/nature.

Author Contributions NBH carried out the experiments in Figs. 1g-h, 2, 3 & 4, and Ext. Data Figs. 2, 3, 4 & 6, and contributed to Figs. 1a-d, 1f & Ext. Data Fig 1. KK carried out experiments in Fig. 1a-f and Ext Data Fig. 1. EK carried out experiments for Ext. Data Fig 5. All authors designed experiments and analysed data. DA and NBH wrote the manuscript. All authors revised the manuscript.

Figure Legends

Figure 1. Ischaemia evokes an inward current in oligodendrocytes by altering K$^+$ fluxes.

a Whole-cell clamped oligodendrocyte. Inset: Alexa dye in processes around an axon. **b** Ischaemia-evoked membrane current in single cell. **c** Current in 179 control cells, 12 cells exposed to 25 µM NBQX and 200 µM D-AP5 from before ischaemia, or 9 cells preloaded[16] with 1 mM PDC. **d** Current (normalised to interleaved control cells) from 8-10 mins after start of ischaemia in cells preloaded with PDC, exposed to NBQX+AP5 throughout ischaemia or from 200 sec after ischaemia starts, or exposed to NBQX or AP5 alone or to zero-Ca^{2+} solution (with 50 µM EGTA) throughout ischaemia. Mann-Whitney p values compare with control cells; cell numbers shown on bars. **e** Effect of Gd^{3+} (100 µM) on ischaemia-evoked current at 8-10 mins (Mann-Whitney p=0.83). **f** I-V relation of 10 cells before and after 5 mins ischaemia (10 mM HEPES internal). **g** Ischaemia-evoked current in 10 cells with 0.5 mM and 9 cells with 50 mM internal HEPES. Ischaemia decreased cell conductance by 2.1$\pm$0.7 nS near -70 mV in 11 cells using 10 mM, and by 2.3$\pm$0.6 nS in 10 cells using 0.5 mM, internal HEPES; 50 mM HEPES abolished the decrease (Fig. 3i). **h** Change of [K$^+$]$_o$ in grey matter (GM, granule cell layer), and in white matter (WM, different slice) with simultaneously recorded oligodendrocyte current. Error bars, s.e.m.

Figure 2. NMDA does not elevate [Ca^{2+}]$_i$ in oligodendrocytes.

a-b Oligodendrocyte membrane current (lower traces, a) and background-subtracted fluorescent dye ratio (R, see Methods, concentration increases are upwards for all dyes) when measuring [Ca^{2+}]$_i$ with Fura-2, [Na$^+$]$_i$ with SBFI, and [K$^+$]$_i$ with PBFI; 100 µM NMDA was applied, or [K$^+$]$_o$ was raised from 2.5 to 5 mM, with fluorescence measured in soma (**a**) or myelinating processes (**b**). Right panels: peak fluorescence change normalised to evoked current (number of cells on bars). **c** NMDA-evoked current and simultaneously recorded [K$^+$]$_o$. **d** Measuring [Ca^{2+}]$_i$ with X-Rhod-1, loaded from pipette or as an acetoxymethyl ester[2], reveals no NMDA-evoked [Ca^{2+}]$_i$ rise. **e** Spontaneous [Ca^{2+}]$_i$ transients in four myelinating processes confirm Fura-2 is working. Error bars, s.e.m.

Figure 3. Ischaemia evokes a $[Ca^{2+}]_i$ and $[Mg^{2+}]_i$ rise gated by internal protons.

a Ratiometric Fluo-4/Alexa-Fluor-594 signals ($[Ca^{2+}]_i$) and membrane potential (Vm) in oligodendrocytes exposed to ischaemia (starting at arrow), or ischaemia in zero $[Ca^{2+}]_o$, or with drugs at concentrations (μM): AP5 50, MK-801 50, 7-chlorokynurenate (7CK) 100, NBQX 25, GABAzine (Gz) 20, TTX 1, Cd^{2+} (to block Ca^{2+} channels) 100. **b** Mean data from experiments like **a** (cell numbers on bars; p values compare with soma or process control values). **c** Data as in a after PDC-preloading or in 0 mM $[K^+]_{bath}$. **d** Ischaemia-evoked $[Mg^{2+}]_i$ rise monitored with Mag-Fluo-4 in normal and Mg^{2+}-free solution. **e** Ischaemia-evoked $[Na^+]_i$ change monitored with SBFI (6 cells). **f** Ischaemia-evoked $[H^+]_i$ rise monitored with BCECF with 0.5 mM and 50 mM internal HEPES (p from Mann-Whitney test). **g** $[K^+]_o$ and oligodendrocyte membrane potential (Vm) with 2.5 or 0 mM $[K^+]_{bath}$, before (Resting) and during ischaemia (Isch peak), and change produced by ischaemia (ΔIsch). **h** Effect of removing K^+ from bath solution on $[H^+]_i$ in control conditions (relative to value at start of K^+ removal), and $[H^+]_i$ increase evoked by ischaemia (normalised to value at start of ischaemia) with 2.5 or 0 mM bath K^+. **i** High $[HEPES]_i$ blocks ischaemia-evoked decrease of membrane conductance. **j-k** Ischaemia-evoked rise of $[Ca^{2+}]_i$ (**j**) and $[Mg^{2+}]_i$ (**k**) are inhibited with 50 mM internal HEPES. **l-m** Uncaging H^+ with light (bars) raises $[Ca^{2+}]_i$ (**l**, an effect reduced by 200 μM IPP or 80 μM HC-030031) and $[Mg^{2+}]_i$ (**m**), but not when caged H^+ is omitted from the pipette. P values in l from Mann-Whitney tests. Error bars, s.e.m.

Figure 4. TRPA1-containing channels mediate ischaemic Ca^{2+} accumulation and myelin damage.

a $[Ca^{2+}]_i$ change (measured with Fluo-4/Alexa-Fluor-594) in soma (black) or processes (white) evoked by TRPA1/TRPV3 agonists (mM): menthol 2, vanillin 1, 2-APB 2, TRPV3 agonists (camphor 2, FPP 0.5) and TRPA1 agonists AITC (0.5), FFA (1) and polygodial (0.2). **b** Rise of $[Ca^{2+}]_i$ evoked by the TRPA1/TRPV3 agonist carvacrol (2 mM, in 1 μM TTX to avoid effects of altered neuronal spiking) is inhibited by the TRPA1/TRPV3 antagonist isopentyl pyrophosphate (IPP, 200 μM, Mann-Whitney test on soma data), the TRPA1

antagonist HC-030031 (80 µM), and by TRPA1 knock-out (Mann-Whitney test on process data), but not by 50 mM internal [HEPES] (p values compare with soma or process control value). **c-d** Ischaemia-evoked $[Ca^{2+}]_i$ rise is blocked by Ruthenium Red (RuR, 10 µM, measured with Fura-2) (**c**), and by La^{3+} (**d**, 1 mM, measured with Fluo-4/Alexa 594, using HEPES-buffered external solution to avoid precipitation, Mann-Whitney test on soma data). **e** Block of ischaemia-evoked $[Ca^{2+}]_i$ rise (measured with Fluo-4) by TRPA1/TRPV3 blocker IPP (200 µM) and by TRPA1 blockers HC-030031 (80 µM) and A967079 (10 µM). Mann-Whitney p values compare with soma or process control values. **f** Ischaemia-evoked $[Ca^{2+}]_i$ rise in wild-type mice, with TRPA1 knocked out (process data showed same trend as the soma but with p=0.07) and with the TRPA1/TRPV3 blocker IPP (200 µM) present in the KO. **g** Ischaemia-evoked $[Ca^{2+}]_i$ rise in wild-type mice, with TRPV3 knocked out and with the TRPA1 blockers HC-030031 (80 µM) and A967079 (10 µM) present in the KO (Mann-Whitney p values). **h** Ischaemia-evoked $[Ca^{2+}]_i$ rise in TRPA1 KO with 10 mM and 50 mM internal [HEPES]. **i** Specimen EM pictures showing control optic nerves and myelin decompaction (white arrows) in nerves exposed to ischaemia or ischaemia in RuR (10 µM), or A967079 (10 µM) and HC-030031 (80 µM) applied together for 60 mins (TRPA1 block). **j-m** Lamella separations (**j**), g ratio (**k**), axon diameter (**l**) and axon vacuoles (**m**: EM picture shows vacuoles (black arrows) forming within axon and periaxonal space during ischaemia) in control, ischaemia alone or ischaemia with RuR (10 µM) or with A967079 (10 µM) and HC-030031 (80 µM) (TRPA1 block). Numbers on bars are 'images (axons)'. P values for j-m from Mann-Whitney tests except l from Kolmogorov-Smirnov test. Error bars, s.e.m.

Methods

Animals

Experiments used Sprague-Dawley rats or transgenic mice of either sex. Animal procedures were carried out in accordance with the guidelines of the UK Animals (Scientific Procedures) Act 1986 and subsequent amendments. TRPV3 knock-out (KO) mice were obtained from JAX (http://jaxmice.jax.org/strain/010773.html). TRPA1 KO mice were obtained as a double knock-out with TRPV1 knocked out (kindly provided by John Wood and Jane Sexton). TRPV1 does not contribute to the ischaemia-evoked $[Ca^{2+}]_i$ rise described here because the TRPV1 antagonist[20,27] capsazepine did not reduce the ischaemia-evoked $[Ca^{2+}]_i$ rise in rat oligodendrocytes (Ext. Data Fig. 6a) and the TRPV1 agonists[20,27] capsaicin (10 µM) and camphor (2 mM) did not evoke a $[Ca^{2+}]_i$ rise (see *Specificity of drugs acting on TRP channels* and Fig. 4a). Wild type and (double) KO mice were obtained from a colony obtained by breeding mice doubly heterozygous for the TRPA1 and TRPV1 knock-outs. The wild-type and KO mice compared share the same doubly heterozygous grandparents.

Brain slice preparation

Cerebellar slices (225 µm thick) were prepared from the cerebellum of P12 rats in ice-cold solution containing (mM) 124 NaCl, 26 NaHCO$_3$, 1 NaH$_2$PO$_4$, 2.5 KCl, 2 MgCl$_2$, 2-2.5 CaCl$_2$, 10 glucose, bubbled with 95% O$_2$/5% CO$_2$, pH 7.4, as well as 1 mM Na-kynurenate to block glutamate receptors. Slices were then incubated at room temperature (21–24°C) in the same solution until used in experiments. Cerebellar slices from P10-17 mice were prepared in ice-cold solution containing (mM) 87 NaCl, 25 NaHC0$_3$, 1.25 NaH$_2$PO$_4$, 2.5 KCl, 7 MgCl$_2$, 0.5 CaCl$_2$, 25 glucose, 75 sucrose, 1 Na-kynurenate and then transferred to the same solution at 27°C and allowed to cool naturally to room temperature. Only 1 cell was recorded from in each slice.

Cell identification and electrophysiology

Oligodendrocytes, cerebellar granule cells and hippocampal pyramidal cells were identified by their location and morphology. All cells were whole-cell clamped with pipettes

with a series resistance of 8-30 MΩ. Electrode junction potentials were compensated. I-V relations were from responses to 200 msec voltage steps. Unless otherwise indicated, cells were voltage-clamped at -74 mV.

External solutions

Slices were superfused with either bicarbonate-buffered solution containing (mM) 124 NaCl, 2.5 KCl, 26 $NaHCO_3$, 1 NaH_2PO_4, 2-2.5 $CaCl_2$, 1 $MgCl_2$, 10 glucose, pH 7.4, bubbled with 95% O_2 and 5% CO_2, or with HEPES-buffered solution containing (mM) 144 NaCl, 2.5 KCl, 10 HEPES, 1 NaH_2PO_4, 2-2.5 $CaCl_2$, 1 $MgCl_2$, 10 glucose, pH set to 7.3 with NaOH, bubbled with 100% O_2. During experiments when NMDA was applied and ion concentration changes were observed with ion sensitive dyes, $MgCl_2$ was omitted from the solution to minimize the Mg^{2+} block. For experiments involving Gd^{3+} and La^{3+}, the HEPES-based solution was used and NaH_2PO_4 was omitted. To simulate ischaemia we replaced external O_2 with N_2, and external glucose with 7 mM sucrose, added 2 mM iodoacetate to block glycolysis, and 25 µM antimycin to block oxidative phosphorylation[31,4]. All ischaemia experiments were done at 33-36°C, while applications of NMDA and of TRP channel agonists were at 24°C. Control and drug conditions were interleaved where appropriate. For calcium imaging experiments when applying ischaemia solution to brain slices from transgenic mice, the experimenter was blind to the genotype.

Intracellular solutions

Cells were whole-cell clamped with electrodes containing either Cs- (to improve voltage uniformity) or K-gluconate-based solution, comprising (mM) 130 Cs-gluconate (or K-gluconate), 2 NaCl, 0.5 $CaCl_2$, 10 HEPES, 10 BAPTA, 2 NaATP, 0.5 Na_2GTP, 2 MgCl, 0.5 K-Lucifer yellow, pH set to 7.2 with Cs- or K-OH (all from Sigma). The K^+-based solution was used for current-clamp experiments. For Ca^{2+} imaging experiments, BAPTA was decreased to 0.01 mM and replaced with 10 mM phosphocreatine, added $CaCl_2$ was reduced to 10 µM, and Lucifer Yellow was replaced with 1 mM Fura-2, or 200 µM Fluo-4 with 50 µM Alexa Fluor 594, or 200 µM X-Rhod-1 with 50 µM Alexa Fluor 488 (all from Molecular

Probes) to allow ratiometric imaging. For imaging pH, Lucifer yellow was replaced with BCECF (96 µM) and the HEPES concentration was decreased to 0.5 mM. This [HEPES] was also used for control experiments when examining the effect of 50 mM internal [HEPES] on the ischaemia-evoked current; ischaemia-evoked membrane current changes were indistinguishable when 0.5 and 10 mM HEPES were used (see main text), presumably because endogenous pH buffering dominates at these low [HEPES] levels. For experiments where the pH-buffering capacity of the internal solution was increased, 68 mM K-gluconate and 50 mM HEPES were used. When uncaging protons, 2 mM 1-(2-nitrophenyl)ethyl sulphate sodium salt (NPE-caged protons, Tocris) was added to the pipette solution and 10 mM HEPES was replaced by 30 mM Tris to prevent UV light-mediated oxidation[32] of HEPES (and K-gluconate was reduced from 130 to 120 mM). For Na^+ and K^+ imaging experiments, Lucifer yellow was replaced with 1 mM of the Na^+-sensing dye SBFI tetra-ammonium salt or of the K^+-sensing dye PBFI tetra-ammonium salt (Molecular Probes). In some experiments MK-801 (1 mM) was added to the internal solution to block NMDA receptors, and cells were depolarised to -10 mV for 10 sec intermittently over a 20 min waiting period to facilitate MK-801 block of open channels.

Single cell ion imaging and H^+ uncaging

For Fura-2, SBFI and PBFI imaging when applying NMDA or during ischaemia, white matter oligodendrocytes and grey matter granule cells were patch-clamped with pipettes containing a solution as described above, fluorescence was excited sequentially at 340±10 nm and 380±10 nm, and emitted light was collected at 510±20 nm. The ratio (R) of the emission intensities (340 nm/380 nm), after subtraction of the background intensity averaged over 4 distant areas of the image, was used as a measure of intracellular ion concentration. Increases of ion concentration generated a fall of fluorescence (F) excited at 380 nm and a rise in fluorescence excited at 340 nm, which is plotted as $\Delta R/R$ in the graphs shown, with R= F_{340nm}/F_{380nm}: an upward deflection corresponds to a rise of concentration of the sensed ion.

For Fura-2, SBFI and PBFI, mean values of R before applying NMDA or ischaemia solution were 0.41 ± 0.05 (n=5), 1.68 ± 0.14 (n=13) and 1.86 ± 1.10 (n=8) respectively.

Fluo-4 and Alexa Fluor 594 were used in the internal solution to measure $[Ca^{2+}]_i$ changes ratiometrically during H^+-uncaging and most ischaemia experiments. To measure $[Mg^{2+}]_i$ Mag-Fluo-4 was used instead of Fluo-4. Fluo-4 (or Mag-Fluo-4) and Alexa Fluor 594 fluorescence were excited sequentially every 2, 10 or 30 seconds at $488\pm10nm$ and $585\pm10nm$, and emission was collected using a triband filter cube (DAPI /FITC/Texas Red, 69002, Chroma). The mean ratio of intensities (F_{488nm}/F_{585nm}) before applying NMDA or ischaemia was 0.81 ± 0.09 (n=16) for Fluo-4 and 0.55 ± 0.04 (n=6) for Mag-Fluo-4. Caged-H^+ were uncaged using 380 ± 20 nm light for 1 second every 2 seconds (repeated 30 times) interspersed with the above excitation wavelengths. BCECF was imaged every 30 seconds at 400 and 480nm, with emission collected using the above tri-band filter. The ratio (R) of the emitted light excited by these two wavelengths (F_{480nm}/F_{400nm}) was used as a measure of $[H^+]_i$ (mean value before ischaemia was 17.6 ± 0.9, n=8) but, since this ratio decreases with increasing $[H^+]_i$, when plotting changes in dR/R in Fig. 3e and Ext. Data Fig. 4 we multiplied them by -1 to produce a trace that increased with $[H^+]_i$.

During ischaemia, slices swelled at the time of the anoxic depolarisation. When cells were patch-clamped with calcium dyes, the resulting movement of the cell away from the electrode sometimes caused $[Ca^{2+}]_i$ oscillations within the cells. These oscillations did not occur if the patch pipette was removed (after 2 minutes to allow dye-filling) before the ischaemic solution was applied. Without the pipette attached to the cell, the time-course of the ischaemia-evoked $[Ca^{2+}]_i$ rise was the same as with the electrode attached, but its amplitude was 69% larger (ratio increase 0.21 ± 0.03, n=20 versus 0.12 ± 0.02, n=16). In some experiments (those in Fig. 4c-g and Ext. Data Fig. 6) we therefore removed the pipette for calcium-imaging.

Control experiments were carried out to check whether the ischaemia-evoked change of pH would affect our $[Ca^{2+}]_i$ measurements. The internal solution for Ca^{2+}-sensing was studied in the experimental bath that the slices usually are placed in. The resting ratio of Fluo-

4 fluorescence to Alexa 594 fluorescence was not significantly affected by altering the pH of the solution from 7.05 to 6.55, and this also did not affect the change of ratio produced by adding 200 nM Ca^{2+} to the sensing solution (Ext. Data Fig. 4b, c). Thus, even a 0.5 unit pH change occurring in the oligodendrocyte would not significantly affect the calcium dye measurements.

AM dye loading

X-Rhod-1-AM (38 μM) dye loading with the myelin marker DIOC6 into P12 cerebellar slices was performed as described previously for optic nerves[2]. Loading times ranged from 1-2 hrs and a de-esterification period of 30 mins at 36°C was allowed before imaging.

Potassium electrodes

Potassium electrodes were made as described[33]. Electrodes were pulled with a resistance of 4-10 MΩ. Electrode tips were silanised by heating them to 250°C for 7 minutes whilst N_2 and N,N-dimethyltrimethylsilylamine (Fluka) were gassed into the tip from the back of the electrode. The tip was then filled with either 6% valinomycin, 1.5% potassium tetrakis(4-chlorophenyl)borate (Fluka) and 92.5% 1,2-dimethyl-3-nitrobenzene (Fluka) or the pre-made potassium sensitive ionophore I – cocktail B (Fluka). The electrodes were back-filled with the bicarbonate-buffered external solution mentioned above (2.5 mM K^+), and attached to a sensitive high resistance electrometer (Model FD 223, World Precision Instruments). A reference electrode tip was placed less than 5 μm away from the K^+ electrode tip, and the voltage changes measured by it were subtracted from those measured with the K^+ electrode. $[K^+]_o$ was determined by calibrating each electrode at the end of every experiment with at least 3 different K^+ concentrations (1, 2.5, 5, 7.5, 10 or 17.5 mM). To check for cross-reactivity, the $[NaCl]_o$ was decreased by 60 mM which led to a -2.2±0.1 mV change in voltage (n=3), while a pH change from 7.3 to 6.5 led to a 0.47±0.22 mV change (n=3). Both of these changes are much less than the 17.5±0.5 mV change (n=18) seen in response to an

increase of $[K^+]_o$ from 2.5 to 5 mM (which is consistent with the electrodes used having an average calibration slope of 60.9 ± 0.9 mV (n=6) per 10-fold change of $[K^+]_o$).

Drugs used

Stock solutions of the following drugs were made up in water: NMDA, AP5, NBQX, MK801, 7-CK, TTX, PDC, IPP, CPG, SKF 96365 and RuR. (S)-MCPG and amiloride were made up in external solution. Carvacrol was made up in ethanol. Bicuculline, bumetanide, HC 030031, A967079, flufenamic acid, capsazepine, FTY720-HCl, 2-APB, AITC, RN1734 and ML204 were made up in DMSO. When used, DMSO and ethanol were also added to control solution at the same concentrations, and did not evoke $[Ca^{2+}]_i$ changes at the concentrations used. Stocks were kept at -20^oC apart from carvacrol, menthol, vanillin, AITC, and RuR, which were made up fresh on each day of use. To minimise evaporation of carvacrol, vanillin and menthol, lids were kept on until the solutions were used. Gd^{3+} and La^{3+} were applied (as chloride salts) in bicarbonate- and phosphate-free solution to avoid chelation by these anions (see External Solutions above).

Immunohistochemical labelling of oligodendrocytes

Cerebellar slices were fixed for 30 mins in 4% PFA, and incubated for 1 to 6 h in 0.1% Triton X-100, 10% goat serum in phosphate-buffered saline at 21°C, then with primary antibody at 4°C overnight with agitation, and then 2 hours or overnight at 24°C with secondary antibody. Primary antibodies were: anti-CC1 (mouse, 1:300, Calbiochem OP80 monoclonal) and anti-Olig-2 (rabbit, 1:700, Millipore, AB9610 polyclonal). Secondary antibodies were: goat anti-rabbit AlexFluor 488 or 568 (Molecular Probes, 1:1000), donkey anti-rabbit AlexFluor 488 (Millipore, 1:1000), and goat anti-mouse Alexa Fluor 568 (Millipore, 1:1000).

Antibody labelling and in situ hybridization for TRPA1 and TRPV3

TRPA1 and TRPV3 antibodies appeared to label the myelinating processes and somata of oligodendrocytes in rat, but the labelling was not significantly different in wild-type mice and mice with TRPA1 or TRPV3 knocked-out (data not shown). We therefore turned to in situ hybridization.

Solutions used for in situ hybridization were pretreated with 0.1% DEPC. Animals were perfused with PBS followed by 4% PFA. Brains were post-fixed in 4% PFA overnight at 4°C, cryoprotected in 20% sucrose overnight at 4°C and frozen in Tissue-Tek O.C.T. Sections (20 μm) collected onto Superfrost Plus microscope slides (VWR International) were hybridized at 65°C overnight with hybridization buffer [50% v/v deionized formamide (Sigma), 10% w/v dextran sulphate (Fluka), 0.1 mg/ml yeast tRNA (Roche), 1x Denhardt's solution (Sigma) and 1x "salts" (200 mM NaCl, 5 mM EDTA, 10 mM Tris-HCl pH 7.5, 5 mM NaH_2PO_4, 5 mM Na_2HPO_4)] containing digoxigenin (DIG)-labelled antisense RNA probe (1:1000). Sections were washed with a washing solution (50% v/v formamide, $1\times$ SSC, 0.1% Tween 20) three times at 65°C for 30 min, followed by two $1\times$ MABT (100 mM maleic acid, 150 mM NaCl, pH 7.5, 0.1% Tween-20) washes at room temperature for 30 min each. Sections were subsequently blocked with blocking solution [2% w/v Blocking Reagent (Roche Diagnostics), 10% v/v heat-inactivated sheep serum (Sigma) in $1\times$ MABT] for 1 h at room temperature and incubated with anti-DIG antibody conjugated with alkaline phosphatase (AP) (Roche Diagnostics, 1:1500 in blocking solution) at 4°C overnight. Sections were then washed in $1\times$ MABT 5 times for 20 min each at room temperature, followed by two 5 min washes in staining buffer (100 mM NaCl, 50 mM $MgCl_2$, 100 mM Tris-HCl, pH 9.5, 0.1% Tween-20). Development was performed at 37°C for 24-48 hours overnight with nitroblue tetrazolium/5-bromo-4-chloro-3-indolyl phosphate in freshly prepared staining solution (50% v/v staining buffer, 25 mM $MgCl_2$, 5% w/v polyvinyl alcohol). Sections were washed in PBS and immunohistochemistry was performed as described above. The plasmids used to generate RNA probes were: IMAGE clone 40129486 for *Trpa1* (linearized with ClaI and transcribed with T3 RNA polymerase) and IMAGE clone 40047664 for *Trpv3* (linearized with XhoI and transcribed with SP6 RNA polymerase). In situ hybridization was repeated using at least three animals for each probe.

Quantifying myelin decompaction during chemical ischaemia using electron microscopy

For chemical ischaemia experiments, optic nerves were dissected from P28 Sprague-Dawley rats and incubated for 1 hour at 36°C in either control or ischaemic solution with and

without the TRPA1/V3 channel blocker ruthenium red (10 µM) or the combined presence of the TRPA1 blockers HC-030031 (80 µM) and A967079 (10 µM). The optic nerves were then immersion fixed in 2% paraformaldehyde and 2% glutaraldehyde in 0.1 M cacodylate buffer overnight. All samples were then post-fixed in 1% OsO_4/0.1 M cacodylate buffer (pH 7.3) at 3°C for 2 hours before washing in 0.1 M cacodylate buffer (pH 7.3). The samples were dehydrated in a graded ethanol-water series at 3°C and infiltrated with Agar 100 resin mix. The nerve was then cut transversely at the mid-point, blocked out and hardened. Ultra-thin sections were taken, 300 microns from the cut end of the middle of the nerve, on a Reichert Ultracut S microtome. Sections were collected on 300 mesh copper grids and stained with lead citrate. The sections were imaged using a Joel 1010 transition electron microscope and a Gatan Orius camera.

In 3 out of 4 experiments the experimenter was blinded to the drug condition prior to imaging (all 4 experiments gave similar results). One section was used from each nerve and eight 21.5 µm x 17.3 µm images were collected at x8000 magnification, four from the peripheral borders of the nerve at 0°, 90°, 180° and 270° positions on the section, and four covering the central portion of the nerve. In all experiments the image identities were then blinded prior to analysis, and the number of large separations of lamellae (decompaction) was counted. Decompaction was defined as a visible white inter-lamellar gap being present between at least 2 normal lamellae. Regions of decompaction were normally separated from each other by an area of compact myelin, but when most of the myelin surrounding an axon had separated lamellae, decompacted regions were counted at 0.5 micron intervals around the sheath. The number of decompacted regions was normalised to the number of axons per image. Some decompaction occurred even in control nerves as a result of the processing for electron microscopy, so we assessed drug block of decompaction by quantifying the ischaemia-evoked increase in decompactions seen without and with the drug present. Myelin g ratios were calculated as the square root of the ratio of the area of the axon to the area of the axon plus myelin sheath. When drawing lines around the axon and sheath, areas of

decompaction were ignored, i.e. we interpolated the lines from regions that were not decompacted. Axon diameter was calculated as $(4.(\text{axon area})/\pi)^{0.5}$. Axon vacuolisation was defined as the inclusion of one or more large (>0.1 µm) empty membrane bound (often circular) organelles within the axon or periaxonal space (Fig. 4m) which may reflect rearrangement of internal axonal membranes or be formed from inclusion of myelin membranes into the axon (Fig. 4m).

Statistics

Data are presented as mean$\pm$s.e.m. Experiments were carried out on brain slices from at least 3 animals on at least 3 separate days, except for a few experiments using expensive drugs which were done on only 2 days. Only 1 cell was recorded from in each slice, so the numbers of cells given are also the numbers of slices. P values are from two tailed Student's t-tests (for normally distributed data, assessed using Shapiro-Wilk tests) or Mann-Whitney U tests (for non-normally distributed data). Normally distributed data were tested for equal variance ($p<0.05$, unpaired F-test) and homo- or heteroscedastic t-tests were chosen accordingly. P values in the text are from unpaired t-tests unless otherwise stated. When small sample sizes ($n\leq4$) achieved $p<0.05$, analysis of sample and effect size typically demonstrated a power for detecting the observed effect of 80-99% (mean 92%), with two exceptions: the process data in Fig. 4c (power 78%) and the soma data in Fig. 4h (power 75%). For multiple comparisons within one experiment (usually one figure panel, but measurements of $[Ca^{2+}]_i$ in somata and processes were treated as separate experiments even when plotted in the same figure panel), P values were corrected using a procedure equivalent to the Holm-Bonferroni method (for N comparisons, the most significant p value is multiplied by N, the 2nd most significant by N-1, the 3rd most significant by N-2, etc.; corrected p values are significant if they are less than 0.05). All statistical analysis was conducted using OriginLab software.

Methods, Supplementary Information and Extended Data References

31. Allen, N.J., Káradóttir, R. & Attwell, D. A preferential role for glycolysis in preventing the anoxic depolarization of rat hippocampal area CA1 pyramidal cells. *J. Neurosci*. **25**, 848-859 (2005).

32. Keynes, R.G., Griffiths, C. & Garthwaite, J. Superoxide-dependent consumption of nitric oxide in biological media may confound in vitro experiments. *Biochem. J.* **369**, 399-406 (2003).

33. Marcaggi, P., Jeanne, M. & Coles, J.A. Neuron-glial trafficking of NH_4^+ and K^+: separate routes of uptake into glial cells of bee retina. *Eur. J. Neurosci.* **19**, 966-976 (2004).

34. Wilke, S., Thomas, R., Allcock, N. Fern, R. Mechanism of acute ischemic injury of oligodendroglia in early myelinating white matter: the importance of astrocyte injury and glutamate release. *J. Neuropathol. Exp. Pathol.* **63**, 872-881 (2004).

35. Kukley, M., Capetillo-Zarate, E. & Dietrich, D. Vesicular release of glutamate from axons in white matter. *Nat. Neurosci.* **10**, 311-320 (2007).

36. Ziskin, J.L., Nishiyama, A., Rubio, M., Fukaya, M. & Bergles, D.E. Vesicular release of glutamate from unmyelinated axons in white matter. *Nat. Neurosci.* **10**, 321-330 (2007).

37. Ye, Z.C., Wyeth, M.S., Baltan-Tekkok, S. & Ransom, B.R. Functional hemichannels in astrocytes: a novel mechanism of glutamate release. *J. Neurosci.* **23**, 3588-3596 (2003).

38. Domercq, M. et al. P2X$_7$ receptors mediate ischemic damage to oligodendrocytes. *Glia* **58**, 730-740 (2010).

39. Friese, M.A. et al. Acid-sensing ion channel-1 contributes to axonal degeneration in autoimmune inflammation of the central nervous system. *Nat. Med.* **13**, 1483-1489 (2007).

40. Feldman, D.H. et al. Characterization of acid-sensing ion channel expression in oligodendrocyte-lineage cells. *Glia* **56**, 1238-1249 (2008).

41. Cavelier, P. & Attwell, D. Tonic release of glutamate by a DIDS-sensitive mechanism in rat hippocampal slices. *J. Physiol.* **564**, 397-410 (2005).

42. Domercq, M. et al. System x_c^- and glutamate transporter inhibition mediates microglial toxicity to oligodendrocytes. *J. Immunol.* **178**, 6549-6556 (2007).

43. Li, Y.H., Han, T.Z. & Meng, K. Tonic facilitation of glutamate release by glycine binding sites on presynaptic NR2B-containing NMDA autoreceptors in the rat visual cortex. *Neurosci Lett.* **432**, 212-216 (2008).

44. Sasaki, A. et al. A mouse model of peripheral postischemic dysesthesia: involvement of reperfusion-induced oxidative stress and TRPA1 channel. *J. Pharmacol. Exp. Ther.* **351**, 368-375 (2014).

45. Moussaieff, A. et al. Protective effects of incensole acetate on cerebral ischemic injury. *Brain Res.* **1443**, 89-97 (2012).

46. Escalera, J., von Hehn, C.A., Bessac, B.F., Sivula, M. & Jordt, S.E. TRPA1 mediates the noxious effects of natural sesquiterpene deterrents. *J. Biol. Chem.* **283**, 24136-24144 (2008).

47. Hu, H. et al. Activation of TRPA1 channels by fenamate nonsteroidal anti-inflammatory drugs. *Pflugers Arch* **459**, 579-592 (2010).

48. Albert, A.P., Pucovsky, V., Prestwich, S.A. & Large, W.A. TRPC3 properties of a native constitutively active Ca2+-permeable cation channel in rabbit ear artery myocytes. *J. Physiol.* **571**, 361-369 (2006).

49. Klose, C. et al. Fenamates as TRP channel blockers: mefenamic acid selectively blocks TRPM3. *Br. J. Pharmacol.* **162**, 1757-1762 (2011).

50. Bang, S., Yoo, S., Yang, T.J., Cho, H. & Hwang, S.W. Farnesyl pyrophosphate is a novel pain-producing molecule via specific activation of TRPV3. *J. Biol. Chem.* **285**, 19362-19371 (2010).

51. Eid, S.R. et al. HC-030031, a TRPA1 selective antagonist, attenuates inflammatory- and neuropathy-induced mechanical hypersensitivity. *Molec. Pain* **4**, 48 (2008).

52. McGaraughty, S. et al. TRPA1 modulation of spontaneous and mechanically evoked firing of spinal neurons in uninjured, osteoarthritic, and inflamed rats. *Molec. Pain* **6**, 14 (2010).

53. Hoffmann, A. et al. TRPM3 is expressed in sphingosine-responsive myelinating oligodendrocytes. *J. Neurochem.* **114**, 654-665 (2010).

54. Ullrich, N.D. et al. Comparison of functional properties of the Ca^{2+}-activated cation channels TRPM4 and TRPM5 from mice. *Cell Calcium* **37**, 267-278 (2005).

55. Miller M et al. Identification of ML204, a novel potent antagonist that selectively modulates native TRPC4/C5 ion channels. *J. Biol. Chem.* **286**, 33436-33446 (2011).

56. Clapham, D.E., Julius, D., Montell, C. & Schultz, G. International union of pharmacology. XLIX. Nomenclature and structure-function relationships of transient receptor potential channels. *Pharmacol. Rev.* **57**, 427–450 (2005).

57. Harteneck, C. & Gollasch, M. Pharmacological modulation of diacylglycerol-sensitive TRPC3/6/7 channels. *Curr. Pharm. Biotech.* **12**, 35-41 (2011).

58. Qin, X. et al. Sphingosine and FTY720 are potent inhibitors of the transient receptor potential melastatin 7 (TRPM7) channels. *Brit. J. Pharmacol.* **168**, 1294-1312 (2013).

59. Vincent, F. et al. Identification and characterization of novel TRPV4 modulators. *Biochem. Biophys. Res. Commun.* **389**, 490-494 (2009).

Extended Data Figure Legends

Ext. Data Fig. 1. Tests for causes of the ischaemia-evoked current.

a Effect of blocking various putative glutamate release mechanisms (blocker concentrations given in Supplementary Information) on peak ischaemia-evoked currents measured in the presence of each drug and in interleaved controls. No significant differences were measured ($p>0.20$). **b** Schematic showing effect of ischaemia-evoked decrease in resting conductance (which is dominated by g_K, left) and ischaemia-evoked $[K^+]_o$ rise (right) on oligodendrocyte membrane current. Black lines are control I-V relations. Red lines are I-V relations in ischaemia showing the effect of a conductance decrease (left) or of a positive shift of reversal potential due to $[K^+]_o$ rising (right). **c** Ischaemia-evoked current change for the two mechanisms in **b** (cf. Fig. 1g). **d** Sum of currents in **c** gives an I-V relation with a reversal potential more negative than E_K. **e** Experimentally observed ischaemia-evoked current in 10 oligodendrocytes with 10 mM internal HEPES (difference of curves in Fig. 1f). Error bars are s.e.m.

Ext. Data Fig. 2. K^+ flux changes generate the oligodendrocyte NMDA-evoked current.

a-b Extracellular Cs^+ (30 mM, replacing Na^+) reduces the inward current evoked by 100 µM NMDA at -74 mV in oligodendrocytes (**a**), but not in hippocampal CA1 pyramidal neurons (**b**). **c-d** Intracellular MK-801 (1 mM) has no effect on NMDA-evoked currents in oligodendrocytes (**c**) but blocks them in pyramidal cells (**d**), while extracellular MK-801 (50 µM) blocks both. **e** Voltage-dependence of the current evoked in 16 oligodendrocytes by 100 µM NMDA and by elevating $[K^+]_o$ from 2.5 to 5 mM. **f** Specimen plot of membrane current in an oligodendrocyte versus local $[K^+]_o$ in response to applying 100 µM NMDA or elevating $[K^+]_o$ from 2.5 to 5 mM. Horizontal cell line shows that if NMDA raises $[K^+]_o$ to (say) 4.5 mM, the current attributable to the $[K^+]_o$ rise alone is 51% of the NMDA-evoked current. Mean value in 11 cells was 49% (see Supplementary Information). Error bars are s.e.m.

Ext. Data Fig. 3. NMDA-evoked ion concentration changes in neurons differ from those in oligodendrocytes

a Specimen records of cerebellar granule cell membrane current and background-subtracted fluorescent dye ratio (R, see Methods) when measuring $[Ca^{2+}]_i$ with Fura-2, $[Na^+]_i$ with SBFI, and $[K^+]_i$ with PBFI, when 100 μM NMDA was applied. The rise of $[K^+]_i$ seen reflects K^+ entry: $[K^+]_{pipette}$ was 32.5 mM, so E_K>-60mV for $[K^+]_o$ >3.3 mM. **b** Mean peak fluorescence change normalised to evoked current (number of cells on bars; p value from Mann-Whitney test). Oligodendrocyte data for comparison are shown in Fig. 2. Error bars are s.e.m.

Ext. Data Fig. 4. Comparison of NMDA-, $[K^+]_{bath}$- and ischaemia-evoked changes of $[H^+]_i$.

a Measurements of changes of ratio (R, see Methods) of background-subtracted BCECF fluorescence in oligodendrocytes in response to 100 μM NMDA and raising $[K^+]_{bath}$ from 2.5 to 5 mM with 0.5 mM internal HEPES, and to ischaemia with 0.5 mM and 50 mM internal HEPES. **b-c** Effect of pH of 10 mM HEPES internal solution on: (**b**) baseline ratio of Fluo-4 to Alexa 594 fluorescence (p value from Mann-Whitney test), and (**c**) change of ratio when [Ca] was increased by 200 nM. Error bars are s.e.m.

Ext. Data Fig. 5. In situ hybridization data on TRP channel expression.

a. In situ data for TRPA1 and TRPV3 in the cerebellum of rats and mice show TRPA1 mRNA in white matter (WM) cells in rats and mice (with denser expression in the adjacent granule cell layer, GCL), but TRPV3 mRNA only in white matter cells in rats. Specimen cells are labelled with white circles. **b** Higher magnification views of white matter, combining in situ hybridization for TRPA1 and TRPV3 with immunocytochemistry for Olig2 (to label oligodendrocyte lineage cells) and CC1 (to define myelinating oligodendrocytes). TRPA1 mRNA is present (in rats and mice) and TRPV3 mRNA is present (in rats but not mice) in myelinating oligodendrocytes (Olig2+, CC1+: arrowheads) and also in some presumed oligodendrocyte precursor cells (Olig2+, CC1-: arrows). **c-d** Quantification of presence of mRNA for TRPA1 (c) and TRPV3 (d) in different oligodendrocyte lineage cell classes.

Numbers on bars are 'images analysed (cells counted)'. P value from Mann-Whitney test. Error bars are s.e.m.

Ext. Data Fig. 6. Further evidence for the identity of TRP channels in oligodendrocytes.

$[Ca^{2+}]_i$ increase (ratio signal from Fluo-4 and Alexa Fluor 594) in oligodendrocyte somata when ischaemia solution was applied with the following drugs present (data normalised to interleaved controls, shown as black bars): RN-1734 (0.5 mM), which blocks[20,59] TRPV4 and, less well, TRPV1, TRPV3 and TRPM8; a cocktail of blockers inhibiting (see Supplementary Information section on *Specificity of drugs acting on TRP channels*) TRPP2, TRPC3, TRPC4, TRPC5, TRPC6, TRPC7, TRPM2, TRPM4, TRPM5, TRPV1, TRPV2, TRPM7, TRPM8 and TRPP1, as well as the store-operated calcium channel component STIM1 and some voltage-gated calcium channels; blocking voltage-gated Ca^{2+} channels with 10μM benidipine; or blocking reversed Na/Ca exchange with 10μM KB-R7943 mesylate (p values, from Mann-Whitney test and t-test as appropriate, were non-significant (p>0.28)). Error bars are s.e.m.

Ext. Data Fig. 7. Schematic of how oligodendrocyte $[Ca^{2+}]_i$ is raised in ischaemia.

Run-down of transmembrane ion gradients leads to glutamate transporters (GluT) reversing (1) and releasing glutamate (2). This depolarizes (and causes a neurotoxic $[Ca^{2+}]_i$ rise in) neurons (3) and raises $[K^+]_o$ (4), causing an inward current (5) through oligodendrocyte K^+ channels (KCh). At the same time, metabolic changes and also the rise of $[K^+]_o$ lead to a rise in oligodendrocyte $[H^+]_i$ (6). This decreases the membrane K^+ conductance (either directly or via TRPA1-containing channels opening) which contributes to the inward current generated, and opens TRPA1-containing channels (7) that let Ca^{2+} and Mg^{2+} into the cell (8). The resulting rise of $[Ca^{2+}]_i$ damages the myelin.
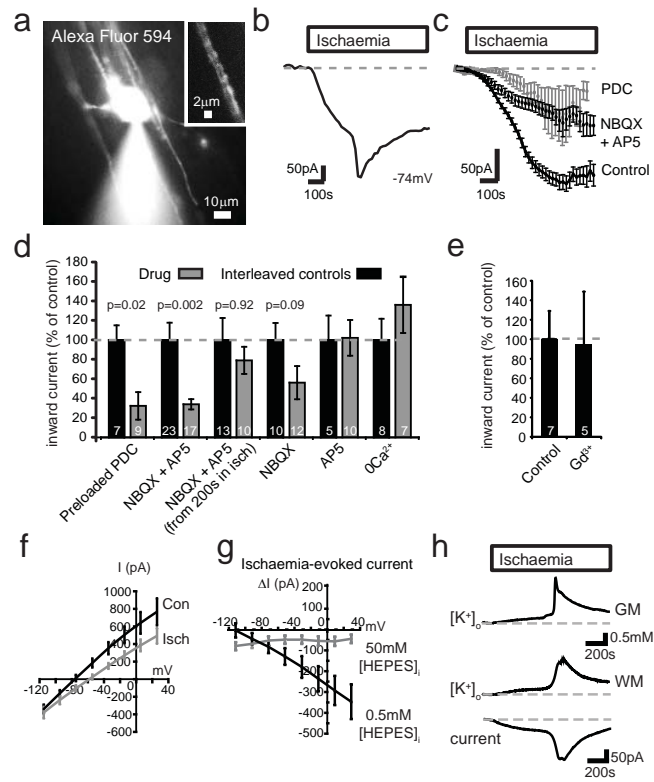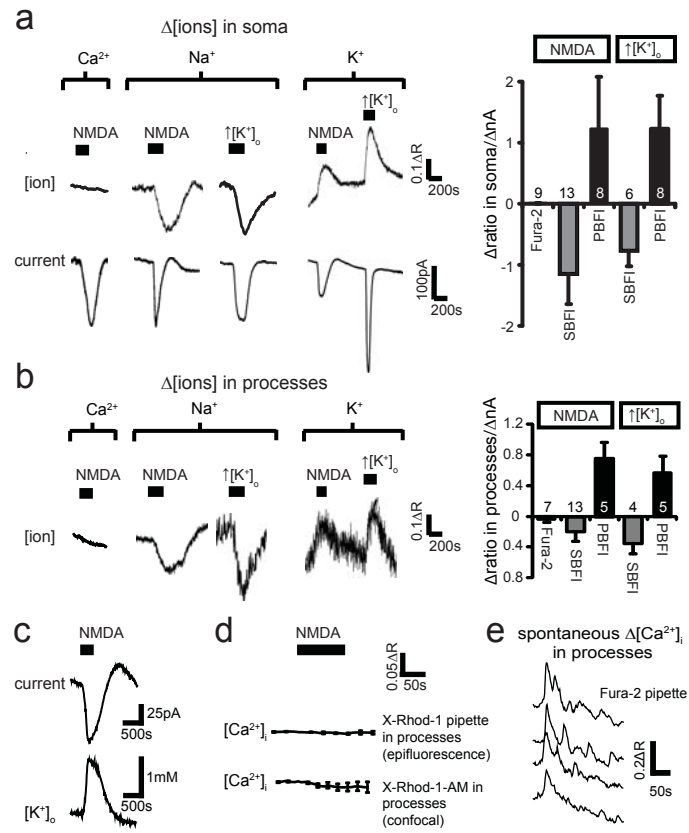
a — Alexa Fluor 594 | 2μm | 10μm

b — Ischaemia | 50pA | 100s | -74mV

c — Ischaemia | PDC | NBQX + AP5 | Control | 50pA | 100s

d — inward current (% of control) | Drug | Interleaved controls | p=0.02 | p=0.002 | p=0.92 | p=0.09 | Preloaded PDC | NBQX + AP5 | NBQX + AP5 (from 200s in isch) | NBQX | AP5 | 0Ca²⁺ | 7 9 23 17 13 10 10 12 5 10 8 7

e — inward current (% of control) | Control | Gd³⁺ | 7 5

f — I (pA) | Con | Isch | mV

g — Ischaemia-evoked current | ΔI (pA) | mV | 50mM [HEPES]ᵢ | 0.5mM [HEPES]ᵢ

h — Ischaemia | [K⁺]ₒ | GM | 0.5mM | 200s | [K⁺]ₒ | WM | current | 50pA | 200s

Fig. 1

a Δ[ions] in soma

Ca²⁺   Na⁺   K⁺

NMDA   NMDA   ↑[K⁺]ₒ   NMDA   ↑[K⁺]ₒ

[ion]

0.1ΔR
200s

current

100pA
200s

Δratio in soma/ΔnA

NMDA   ↑[K⁺]ₒ

2

1

9   13   8   6   8

Fura-2   SBFI   PBFI   SBFI   PBFI

-1

-2

b Δ[ions] in processes

Ca²⁺   Na⁺   K⁺

NMDA   NMDA   ↑[K⁺]ₒ   NMDA   ↑[K⁺]ₒ

[ion]

0.1ΔR
200s

Δratio in processes/ΔnA

NMDA   ↑[K⁺]ₒ

1.2

0.8

0.4

7   13   5   4   5

Fura-2   SBFI   PBFI   SBFI   PBFI

0.4

0.8

c

NMDA

current

25pA
500s

[K⁺]ₒ

1mM
500s

d

NMDA

0.05ΔR
50s

[Ca²⁺]ᵢ   X-Rhod-1 pipette
in processes
(epifluorescence)

[Ca²⁺]ᵢ   X-Rhod-1-AM in
processes
(confocal)

e spontaneous Δ[Ca²⁺]ᵢ
in processes

Fura-2 pipette
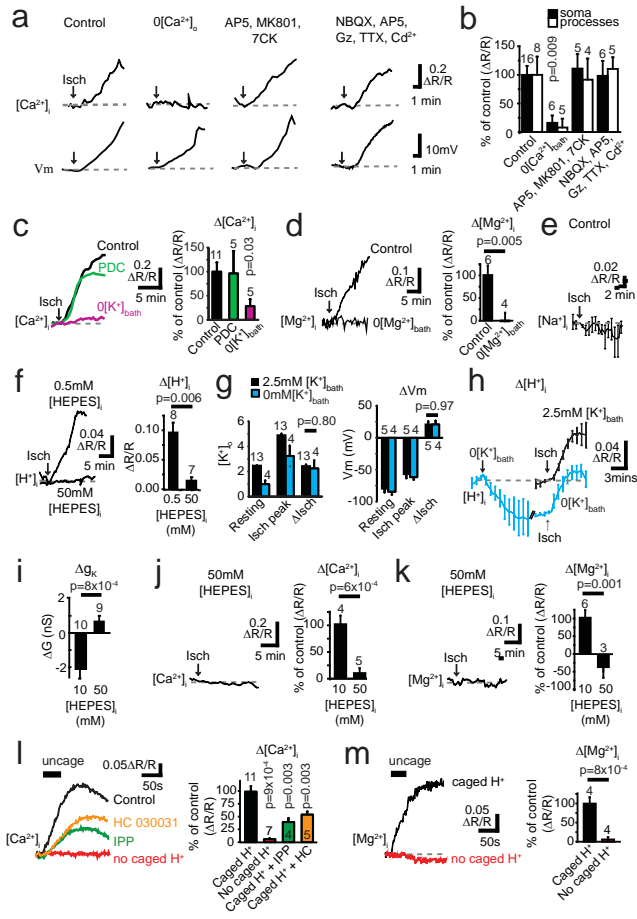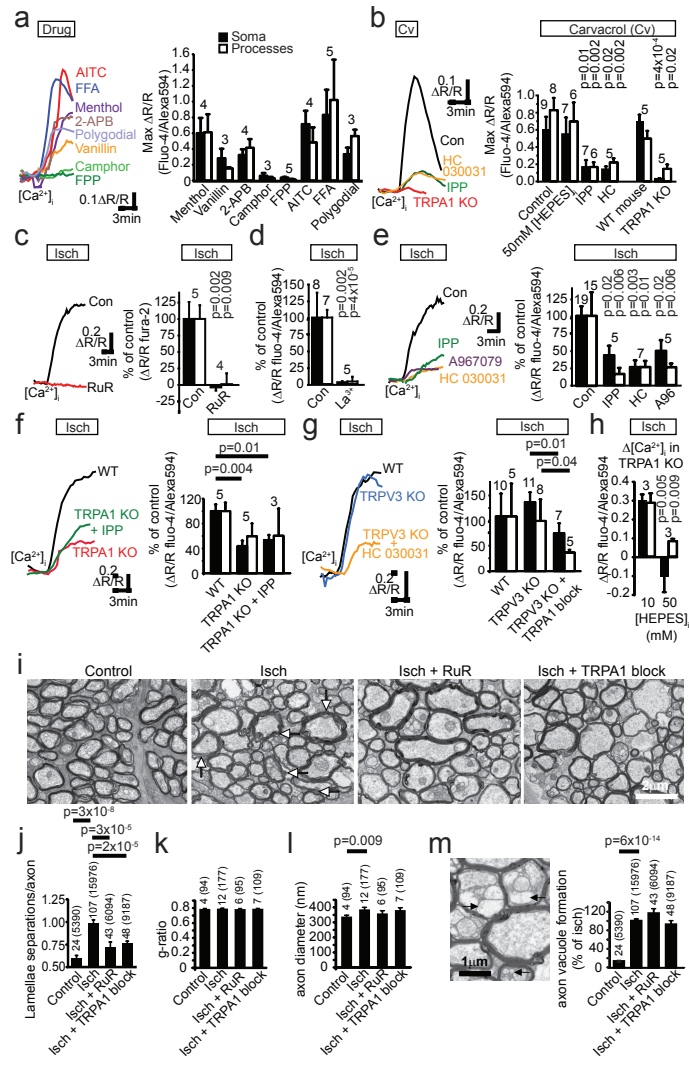
0.2ΔR
50s

Fig. 2

Fig. 3

Fig. 4

<center>**Supplementary Information**</center>

Effect of internal cation on the ischaemia-evoked inward current in oligodendrocytes

The peak inward current evoked by ischaemia (and its waveform) was not significantly different with Cs^+ or K^+ as the main pipette cation (209 ± 10 pA, n=179, and 191 ± 41 pA, n=10, respectively, p=0.67).

Effect of blocking potential glutamate release mechanisms

In contrast to the suppressive effect of blocking glutamate release by reversed uptake, blocking other candidate mechanisms for glutamate release (from before the onset of ischaemia) did not affect the inward current significantly. Ext. Data Fig. 1a shows that there was no significant effect, when compared with interleaved control cells, on the peak ischaemia-evoked current of application of: 50 μM bumetanide to inhibit NKCC1 transporters and prevent swelling of astrocytes leading to glutamate release[34]; 100 μM $CdCl_2$ to prevent exocytotic glutamate release driven by Ca^{2+} entry through voltage-gated Ca^{2+} channels[35,36]; 100 μM lanthanum ($LaCl_3$) to block glutamate release through gap junctional hemichannels[37]; 10 μM BBG to block $P2X_7$ receptors[38]; 100 μM amiloride to block ASIC channels which may be activated by the acid shift occurring in ischaemia[39,40]; 1 μM TTX to block action potential driven glutamate release[35,36]; 100 μM bicuculline to block $GABA_A$ receptors, 1 mM MCPG to block mGluRs, or 50 μM CPG ((S)-4-carboxyphenylglycine) to block glutamate release by cystine-glutamate exchange[41,42].

Contribution of $[K^+]_o$ rise and g_K decrease to the ischaemia-evoked inward current

We assumed that the ischaemia-evoked current reflects the sum of the current produced by a rise of $[H^+]_i$ suppressing a mainly K^+-specific ohmic conductance with a conductance of 2.3 nS (the slope of the 0.5 mM HEPES line in Fig. 1g; the change of current this produces is schematised in Ext. Data Fig. 1b left panel), and a voltage-independent inward current of -58 pA (the mean value of the 50 mM HEPES data in Fig. 1g) produced by the rise of $[K^+]_o$ shifting the Nernst potential for K^+ (the change of current this produces is schematised in Ext. Data Fig. 1b right panel). Together, these changes are expected to generate an ischaemia-evoked current which shows a conductance decrease and an apparent reversal potential more negative than the original value of E_K (Ext. Data Fig. 1c-d) as

is seen experimentally (Ext. Data Fig. 1e). For a mean input resistance of 148 ± 23 MΩ in 10 cells, this analysis implies that, on average, ischaemia reduced the resting conductance of the cell by 34%. Since the total inward current generated at -74 mV by the conductance decrease and the $[K^+]_o$ rise was 85 pA (Fig. 1f) and 58 pA of this was generated by the $[K^+]_o$ rise, it follows that the conductance decrease generated 27 pA of inward current. Thus, the conductance decrease produced 32%, and the $[K^+]_o$ rise produced 68% of the inward current at -74mV (at more positive potentials the contribution of the conductance decrease will be larger).

A $[K^+]_o$ rise and K^+ influx mediate much of the response to NMDA

Since both ischaemia and application of glutamate or NMDA are expected to depolarize cells and release $[K^+]_o$, we compared the effects of 100 μM NMDA application to those of a small elevation of $[K^+]_o$. The oligodendrocyte response to a 2.5 mM elevation of $[K^+]_o$ was strikingly similar to the response to NMDA, with a decrease of $[Na^+]_i$ and an elevation of $[K^+]_i$ (Fig. 2a, b) and no significant change in $[Ca^{2+}]_i$ (-0.001$\pm$0.010 change in R, p=0.36). The I-V relation of both the NMDA and K^+-evoked currents decreased towards zero above +25 mV (Ext. Data Fig. 2e). Consistent with a $[K^+]_o$ rise-evoked K^+ influx mediating a substantial part of the NMDA-evoked current, applying 30 mM external Cs^+ to block oligodendrocyte K^+ channels reduced the NMDA-evoked current in oligodendrocytes by 88% (p=0.03, 7 cells), while having no effect on the NMDA-evoked current in hippocampal pyramidal cells (Ext. Data Fig. 2a, b). Conversely, including 1 mM MK-801 in the pipette to block NMDA receptors from the inside[43] (and waiting 20 mins to allow the drug to diffuse through the cell) reduced the NMDA-evoked current in pyramidal cells by 88% (p=0.003, n=6), while having no effect on that in oligodendrocytes (Ext. Data Fig. 2c, d). Although this lack of effect might theoretically reflect the NMDA receptors in oligodendrocytes having an unusual subunit composition[4] which is not susceptible to block by internal MK-801, this is not likely because they are blocked by external MK-801 (Ext. Data Fig. 2c).

Using an extracellular K^+-sensitive microelectrode to assess the $[K^+]_o$ rise occurring near the patch-clamped oligodendrocyte when NMDA or an increase in $[K^+]_o$ were applied (Fig. 1h), we found that 100 μM NMDA raised the local $[K^+]_o$ by 1.52 ± 0.17 mM (n=19), while switching from 2.5 mM to 5 mM $[K^+]$ in the bath superfusate raised the local $[K^+]_o$ by 2.32 ± 0.18 mM near 21 cells. Plots of the

membrane current change against local $[K^+]_o$ during these responses (Ext. Data Fig. 2f) in 11 cells showed that the inward membrane current increased approximately linearly with the rise of $[K^+]_o$, with a slope that was 51% smaller (p=0.03) when increasing $[K^+]$ in the superfusate (-61.2 ± 19.3 pA/mM) than when applying NMDA (-124.0 ± 46.1 pA/mM). These data suggest that a rise of $[K^+]_o$ is responsible for 49% of the inward current, although the percentage could be significantly larger since the oligodendrocyte membrane is presumably closer than the K^+-sensing electrode to the source of K^+ when NMDA is applied than when the superfusate $[K^+]$ is raised.

Specificity of drugs acting on TRP channels

Both TRPA1 and TRPV3 have previously been suggested to play a role in the response of the CNS to ischaemia[44,45]. Unfortunately the pharmacology of TRP channels is complex, with many drugs acting non-specifically on different channels. Our conclusion that TRPA1 is the major contributor to raising $[Ca^{2+}]_i$ in ischaemia is based on the following logic.

(1) The ischaemia-evoked $[Ca^{2+}]_i$ rise is abolished by removal of external Ca^{2+} and so reflects entry through an ion channel (Fig. 3a).

(2) The general TRP channel blockers ruthenium red and La^{3+} block the ischaemia-evoked $[Ca^{2+}]_i$ rise (Fig. 4c-d), suggesting the involvement of a TRP channel.

(3) Other known intracellular targets of ruthenium red, such as ryanodine receptors and the mitochondrial uniporter, are unlikely to explain the actions of ruthenium red because, as stated above, the $[Ca^{2+}]_i$ rise reflects Ca^{2+} entry from the extracellular space.

(4) Voltage-gated Ca^{2+} channels, which are also targeted by ruthenium red and La^{3+}, are not the source of the ischaemia-evoked $[Ca^{2+}]_i$ rise since neither Cd^{2+} (Fig, 3b) nor benidipine (Ext. Data Fig. 6a) blocked the rise, and these channels are not Mg^{2+}-permeable while ischaemia evokes entry of Mg^{2+} through the H^+-gated channel (Fig. 3d, k).

(5) The ischaemia-evoked $[Ca^{2+}]_i$ rise is abolished (Fig. 3j) by reducing the ischaemia-evoked rise of $[H^+]_i$ with a pH buffer (Fig. 3f), and so reflects entry through a H^+-gated channel.

(6) Of the TRP channels, only TRPA1 and TRPV3 are currently known to be activated by intracellular protons[20,23,24].

(7) Drugs that activate TRPA1 but not TRPV3 (polygodial, AITC, FFA), or that activate both TRPA1 and TRPV3 (menthol, vanillin, carvacrol, 2-APB), but not drugs that activate TRPV3 and not TRPA1 (FPP, camphor), elevate $[Ca^{2+}]_i$ (Fig. 4a, b). The most specific TRPA1 agonist is polygodial which does not act[46] on TRPV1, TRPV2, TRPV3, TRPV4 or TRPM8, followed by AITC (allyl-isothiocyanate) which also acts[20] on TRPV1. Flufenamic acid activates TRPA1 but inhibits TRPV1 and TRPV3[47] and also acts on[20,27,47-49] TRPC3, TRPC5, TRPC6, TRPC7, TRPV4, TRPV5, TRPV6, TRPM2, TRPM3, TRPM4, TRPM5 and TRPM8. Carvacrol activates TRPA1 and TRPV3, and inhibits TRPM7[20,27]. Farnesyl pyrophosphate (FPP) activates TRPV3 but does not activate TRPV1, TRPV2, TRPV4, TRPA1, and TRPM8[25,50]. Camphor activates TRPV3, activates TRPV1 and TRPM8, and inhibits TRPA1[20,27]. Agonists for other TRPs (including 10 μM capsaicin[20,27] for TRPV1, 5 cells, not shown) did not raise $[Ca^{2+}]_i$ detectably. Thus, activation of TRPA1, but not of TRPV3, raises oligodendrocyte $[Ca^{2+}]_i$.

(8) The $[Ca^{2+}]_i$ rise evoked by carvacrol (a TRPA1 and TRPV3 agonist, and TRPM7 blocker[20,27]) is blocked by the TRPA1/TRPV3 antagonist[25] isopentenyl pyrophosphate (IPP), by the specific TRPA1 antagonist[51] HC-030031, and by TRPA1 knock-out (Fig. 4b). HC-030031 blocks TRPA1 without affecting TRPV1, TRPV3, TRPV4, TRPM8 or 48 other receptors, transporters and enzymes[51]. Thus, the blocker pharmacology matches that of the activator pharmacology.

(8) Isopentenyl pyrophosphate and HC-030031 also reduce the $[Ca^{2+}]_i$ rise evoked by uncaging of protons in oligodendrocytes (Fig. 3l), implying that TRPA1 is the main contributor to this response.
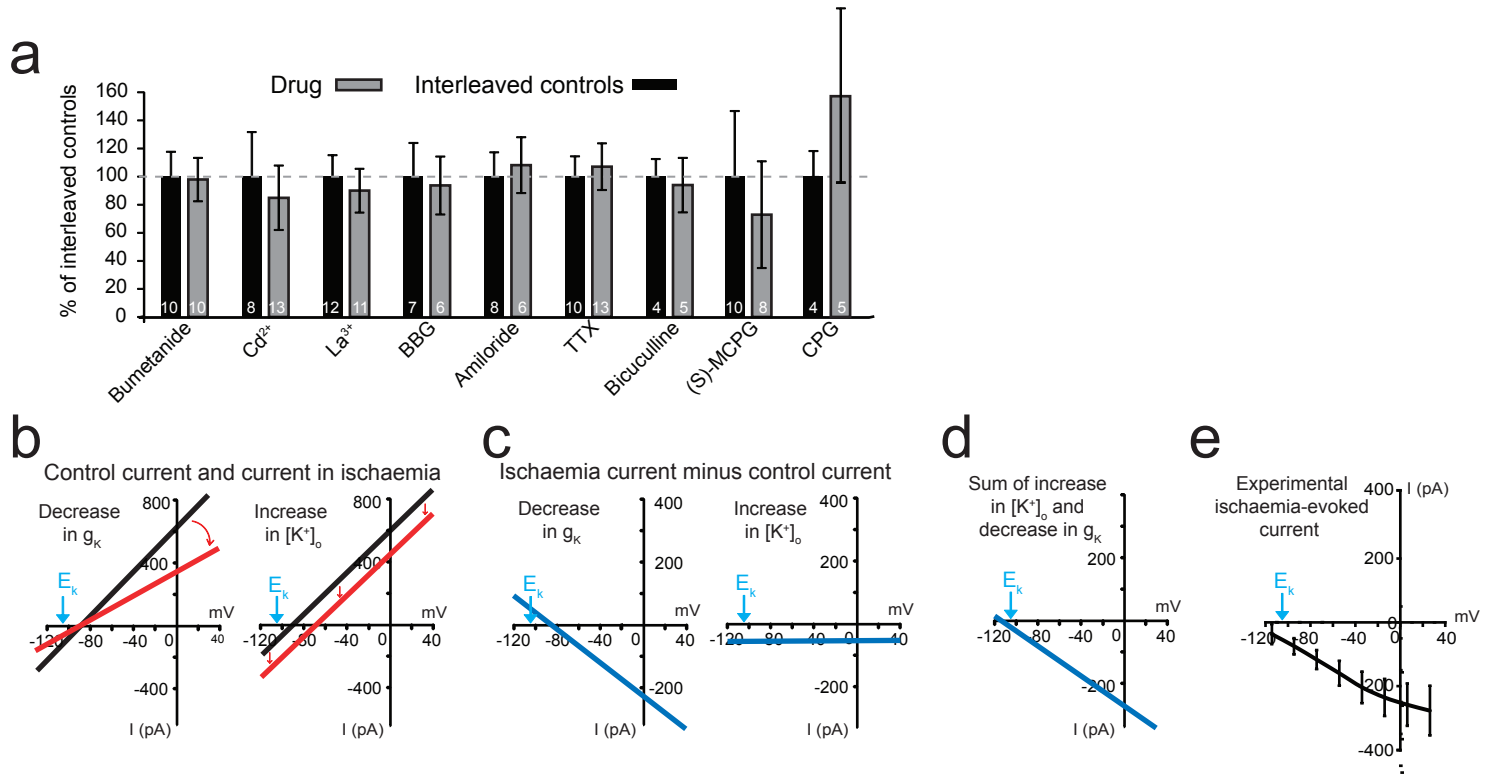
(9) The specific TRPA1 blockers[51,52] HC-030031 and A967079 greatly reduced the ischaemia-evoked $[Ca^{2+}]_i$ rise (Fig. 4e). HC-030031 blocks TRPA1 without affecting TRPV1, TRPV3, TRPV4, TRPM8 or 48 other receptors, transporters and enzymes[51]. A967079 has minimal activity at 89 different G-protein-coupled receptors, enzymes, transporters, and ion channels including other TRP channels[52].
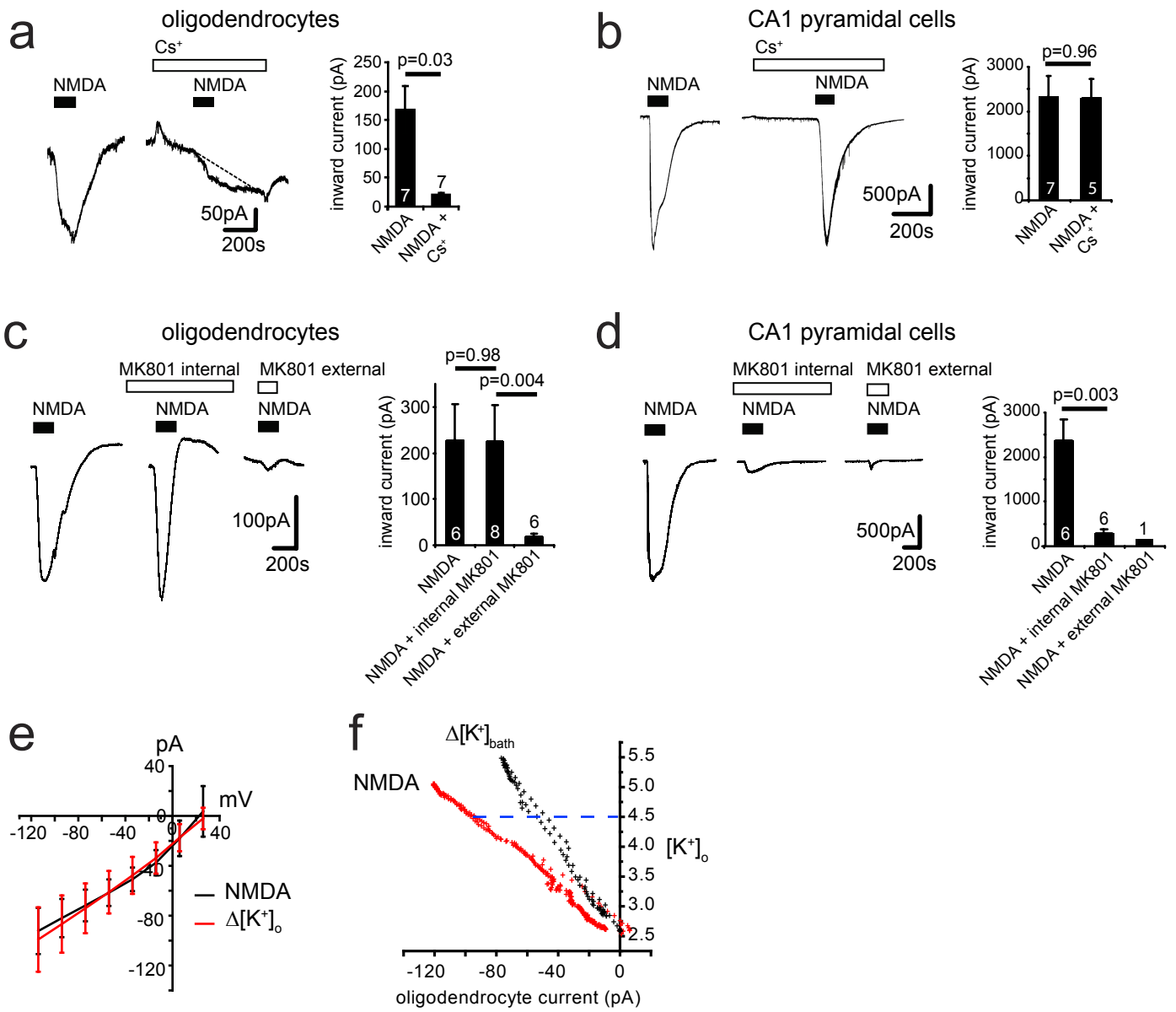
(10) TRPA1 knock-out, but not knock-out of TRPV3, slowed and greatly reduced the ischaemia-evoked $[Ca^{2+}]_i$ rise (Fig. 4f, g). To check for mistakes in our understanding, we applied the TRPA1/TRPV3 blocker IPP in the TRPA1 KO and (as expected) it had no effect, and we applied the TRPA1 blocker HC-030031 in the TRPV3 KO and (as expected) it greatly reduced the ischaemia-evoked $[Ca^{2+}]_i$ rise.
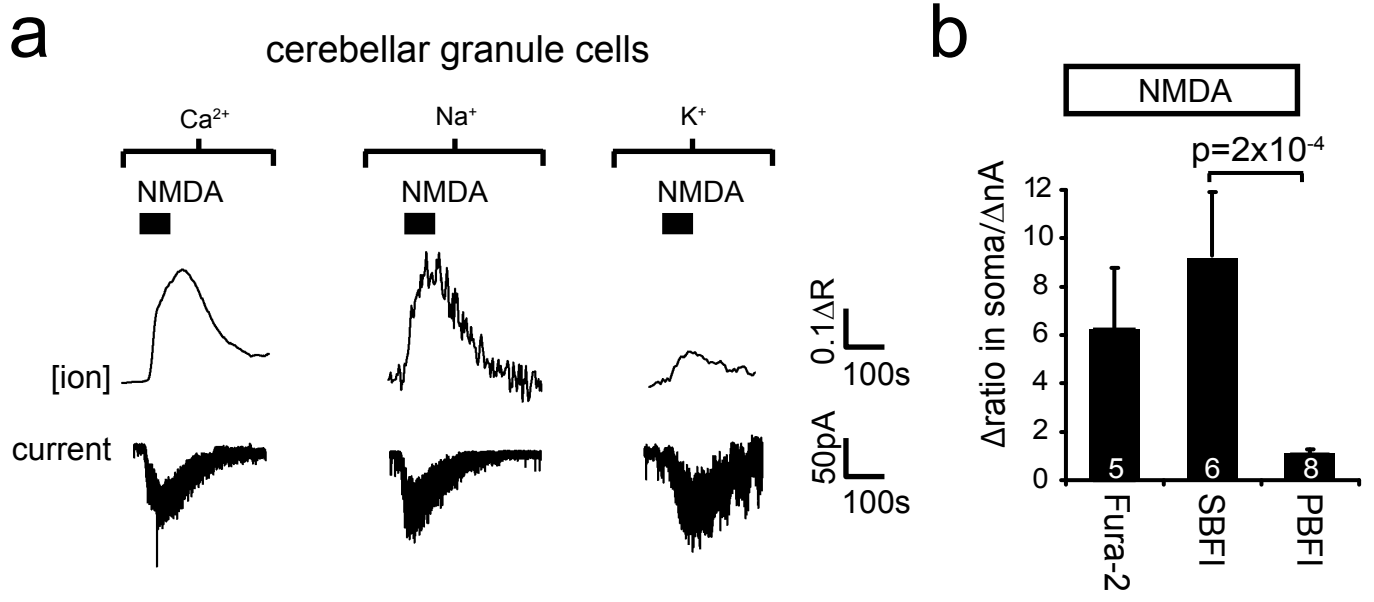
(11) Myelin damage was reduced by the specific TRPA1 blockers HC-030031 and A967079 (Fig. 4i-j).
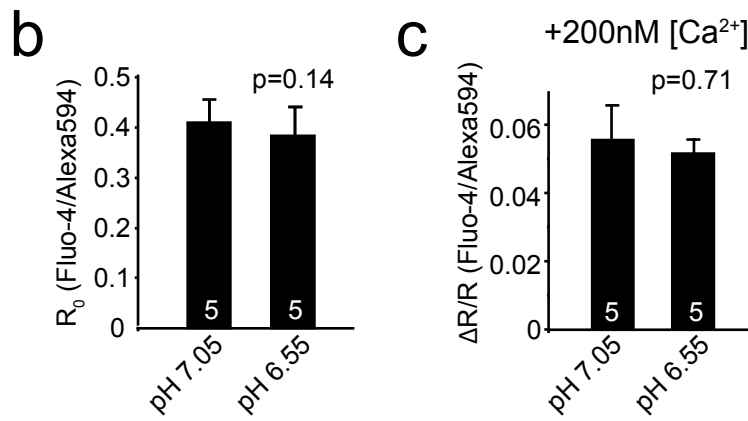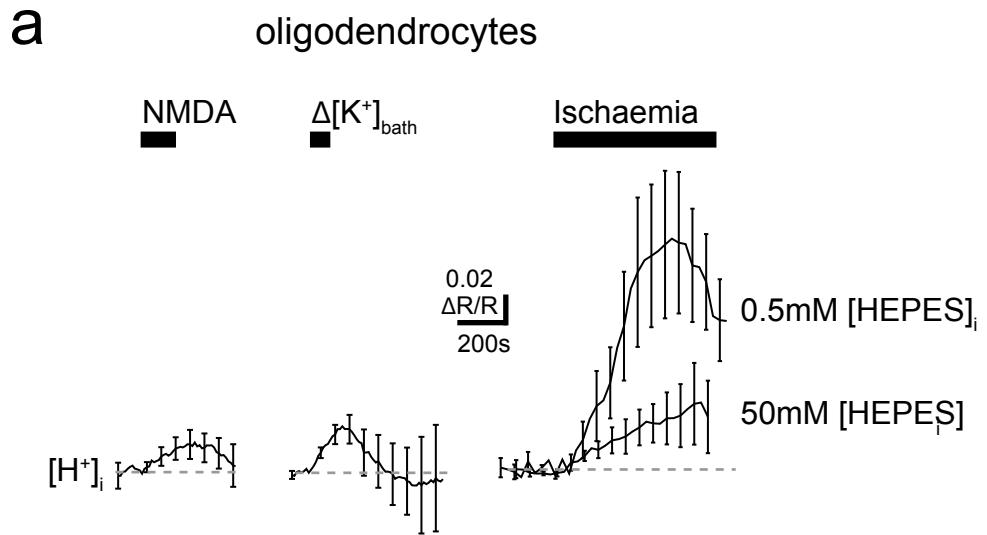
(12) The only TRP channel previously reported to be present in oligodendrocytes is TRPM3, which acts as a sphingosine-gated Ca^{2+}-channel[53]. However, when we applied sphingosine (50 μM) it evoked no significant increase in $[Ca^{2+}]_i$ (ΔR/R = 0.014±0.012, n=5, p=0.16).

(13) The ischaemia-evoked $[Ca^{2+}]_i$ increase was not inhibited (p>0.53, Ext. Data Fig. 6a) by agents blocking TRP channels other than TRPA1, as follows: flufenamic acid (250 μM) which blocks[27,54] TRPP2, TRPC3, TRPC5, TRPC7, TRPM2, TRPM4 and TRPM5; ML204 (20 μM) which blocks[20,55] TRPC4 and TRPC5; SKF-96365 (100 μM) which blocks[27,56,57] TRPV2, TRPC3, TRPC6, TRPC7 and TRPP1, as well as the store-operated calcium channel component STIM1 and some voltage-gated calcium channels; capsazepine (CPZ, 100 μM) which blocks[20] TRPV1 and TRPM8; FTY720 (1 μM) which blocks[58] TRPM7; RN-1734 which blocks[59] TRPV4.

a

Drug ▨   Interleaved controls ▬

Bumetanide Cd²⁺ La³⁺ BBG Amiloride TTX Bicuculline (S)-MCPG CPG

b Control current and current in ischaemia

Decrease in g_K Increase in $[K^+]_o$

c Ischaemia current minus control current

Decrease in g_K Increase in $[K^+]_o$

d Sum of increase in $[K^+]_o$ and decrease in g_K

e Experimental ischaemia-evoked current

Ext. Data Fig. 1

a   oligodendrocytes

b   CA1 pyramidal cells

c   oligodendrocytes

d   CA1 pyramidal cells

e

f

Ext. Data Fig. 2

a cerebellar granule cells

Ca²⁺ Na⁺ K⁺

NMDA NMDA NMDA

[ion]

current

0.1ΔR
100s

50pA
100s

b

NMDA

p=2x10⁻⁴

Δratio in soma/ΔnA

Fura-2 SBFI PBFI

Ext. Data Fig. 3

a

oligodendrocytes

NMDA $\Delta[K^+]_{bath}$ Ischaemia

0.02
$\Delta R/R$
200s

0.5mM $[HEPES]_i$

50mM $[HEPES]_i$

$[H^+]_i$

b

R_0 (Fluo-4/Alexa594)

p=0.14

5   5

pH 7.05   pH 6.55

c

+200nM $[Ca^{2+}]$

$\Delta R/R$ (Fluo-4/Alexa594)

p=0.71

5   5

pH 7.05   pH 6.55

Ext. Data Fig. 4

Ext. Data Fig. 5

oligodendrocytes

Legend: Interleaved controls ■ (black), Drug ■ (gray)

Y-axis: % of interleaved controls ($\Delta R/R$ Fluo-4·Alexa594)

X-axis categories: RN-1734; CPZ, ML204, SKF, FTY, FFA; Benidipine; KB-R7943

Bar values (n): RN-1734: 3, 3; CPZ, ML204, SKF, FTY, FFA: 6, 4; Benidipine: 5, 6; KB-R7943: 8, 5

Ext. Data Fig. 6

Ext. Data Fig. 7